

Spin injection and perpendicular spin transport in graphite nanostructures

T. Banerjee^{*1,2,3}, W.G. van der Wiel² and R. Jansen³

¹ *Physics of Nanodevices,
Zernike Institute for Advanced Materials,
University of Groningen, The Netherlands*

² *Nanoelectronics Group,
MESA⁺ Institute for Nanotechnology,
University of Twente, The Netherlands*

³ *MESA⁺ Institute for Nanotechnology,
University of Twente, The Netherlands*

**e-mail: T.Banerjee@rug.nl*

Abstract

Organic and carbon-based materials are attractive for spintronics because their small spin-orbit coupling and low hyperfine interaction is expected to give rise to large spin-relaxation times. However, the corresponding spin-relaxation length is not necessarily large when transport is via weakly interacting molecular orbitals. Here we use graphite as a model system and study spin transport in the direction perpendicular to the weakly bonded graphene sheets. We achieve injection of highly (75%) spin-polarized electrons into graphite nanostructures of 300-500 nm across and up to 17 nm thick, and observe transport without any measurable loss of spin information. Direct visualization of local spin transport in graphite-based spin-valve sandwiches also shows spatially uniform and near-unity transmission for electrons at 1.8 eV above the Fermi level.

PACS numbers: 85.75.-d, 73.63.-b, 75.76.+j, 72.25.Rb.

The efficient injection and transport of spin-polarized carriers in electronic nanostructures is a subject of intense research and a basic ingredient of spintronics, a technology in which digital information is represented by spin [1, 2]. Organic and carbon-based materials are attractive for spintronics because spin is only weakly coupled to other degrees of freedom in these materials, leading to favorably long spin-relaxation times [3–5]. Indeed, successful spin transport through organic materials [6–12], carbon nanotubes [13–15] and graphene [16–18] has recently been reported. Yet, the understanding of injection and transport of spin-polarized carriers in organic materials is still at its infancy [4, 5], and explicit confirmations of very large spin-relaxation lengths remain scarce. For instance, spin transport through Alq_3 (tris-(8-hydroxyquinoline) aluminium) was reported to decay with a characteristic length of 10 to 40 nm at low temperature [7, 9, 12], whereas a length scale of 13 nm was observed for amorphous rubrene [10]. The spin-flip length in the organic semiconductor CuPc (copper phthalocyanine) was found to be 10 to 30 nm [11]. For comparison, the spin-diffusion length in silicon was recently determined to be 200 to 300 nm at room temperature [19], and larger values have been obtained at room temperature in graphene [16].

Although a large spin *lifetime* is desirable, the corresponding spin-relaxation *length* is not always large, because it is also determined by transport parameters (such as the carrier mobility and the diffusion constant). These are equally important. Transport in most organic compounds is complicated by the rather localized nature of the electronic states derived from weakly interacting molecular orbitals. Consequently the description of spin diffusion and relaxation for hopping-like conduction is under debate [4, 5, 20]. On the other hand, carbon nanotubes and graphene exhibit band conduction with high carrier mobility. Graphite, with its anisotropic resistivity [21], forms an interesting system that combines the different transport regimes. The conductivity is large within the plane of the graphene sheets enabled by highly delocalized electronic states. However, in the direction perpendicular to the carbon sheets the π orbital overlap is limited, and the conductivity and mobility are at least two orders of magnitude smaller. Transport in this direction thus resembles that found in many organic materials, and hence graphite is a unique system to study spin transport across interfaces with weak electronic interactions.

Our experiment thus involves a spin-valve sandwich consisting of two ferromagnetic metal layers and a graphite spacer. The first ferromagnet acts as a spin filter, producing a spin-polarized current that is subsequently injected into the graphite. After transmission of

the graphite, the electrons proceed into the second ferromagnet that acts as analyzer of the transmitted spin polarization. When spin is conserved in the graphite spacer, the total transmission is largest when the magnetization of the two ferromagnets is aligned parallel (P), and smaller for antiparallel (AP) alignment. One obtains a magnetocurrent $MC = (I^P - I^{AP})/I^{AP}$, where I^P and I^{AP} denote the transmitted current for the P and AP magnetic state, respectively. Spin relaxation in the graphite spacer tends to equalize I^P and I^{AP} and reduces the MC. Comparing the MC for structures with different graphite thickness thus provides information on the spin relaxation in the graphite spacer.

We employ Ballistic Electron Magnetic Microscopy [22–24] (BEMM, see Fig. 1a), which is uniquely suited to study perpendicular spin transport through buried layers and their interfaces [25, 26]. The technique is based on scanning tunneling microscopy (STM) and provides direct visualization of any nanoscale spatial inhomogeneity of the transport, which has always been an issue for the interpretation of magnetoresistive measurements particularly for spin valves with organic spacers [5]. Another feature of BEMM is that the electron energy can be varied, typically between 0.3 and 2 eV, giving valuable information on (spin-) transport and fundamental excitations not accessible by ordinary conduction at the Fermi energy. We use BEMM to demonstrate perfect transmission of spin-polarized electrons perpendicularly through graphite nanostructures of up to 17 nm thick, corresponding to 51 sheets of graphene. The graphite nanoflakes are prepared by sonication of exfoliated flakes of HOPG (SPI-2 grade, density 2.27 g/cm³, resistivity of 4×10^{-5} Ωcm within the plane, and 1.5×10^{-1} Ωcm perpendicular to the plane) in VLSI-grade isopropyl alcohol. Characterization by atomic force microscopy (see Fig. 1b and c) shows that the flakes are typically around 10 nm in height with a few being as high as 20 nm. Their lateral dimension is between 100 and 500 nm. The graphite flakes are randomly distributed over the surface, where an area of 5×5 μm² on average contains a few nanoflakes that can be located without extensive searching.

For the BEMM experiments, we start with an n-type Si(100) substrate (resistivity 5–10 Ωcm) having a 300 nm thick SiO₂ with circular contact holes of 150 μm diameter. After a final etch in HF acid to remove any native oxide, metal layers were deposited by thermal evaporation using a molecular beam epitaxy system (base pressure 10^{-10} mbar). First, a 8 nm Au layer was evaporated to form a Au/Si Schottky barrier, followed by 3 nm of Ni₈₀Fe₂₀ and 3 nm of Au, the latter providing a chemically inert cap layer. The sample was then

taken out of the deposition chamber for *ex situ* transfer of the graphite nanoflakes. Using a micro-syringe, the nanoparticle solution is dispersed onto the Si/Au/Ni₈₀Fe₂₀/Au template and the solvent is allowed to dry, leaving graphite nanoflakes behind. The sample was then re-introduced into the deposition system and a stack of Au(3nm)/Co(3nm)/Au(4nm) was evaporated.

The final structure consists of regions without any graphite, and regions with a graphite nanoflake sandwiched between two ferromagnetic layers via intermediate layers of Au (see Fig. 1a). The STM tip that is used to inject current into the structure can then be positioned in a location with or without graphite (location (1) and (2), respectively). The resulting transmission and MC can thus be compared directly. For all measurements, the metal surface of the sample is grounded and negative voltage V_T is applied to the STM tip with the tunnel current I_T kept constant using feedback. The energy of the injected electrons is given by eV_T and transport in the metal/graphite sandwich is thus by hot electrons [27]. Before reaching the graphite, the electrons are spin filtered in the Co metal layer that preferentially transmits hot electrons of majority spin due to spin-dependent scattering [27, 28]. A 3 nm thick Co film is known to transmit hot electrons that have 75% spin polarization [27, 28]. After injection and transport through the graphite and spin analysis in the second ferromagnetic layer, the transmitted electrons are collected in the conduction band of the n-type Si substrate having a separate (third) electrical contact. Collection in the Si is possible only [25, 26] for those electrons that have retained sufficient energy and the proper momentum to cross the 0.8 V high Schottky barrier at the Au/Si interface, making the collected current I_C sensitive to scattering during transport in the graphite sandwich. All BEMM measurements were performed at 150 K using PtIr metal tips. Details of the BEMM setup have been described elsewhere [24, 29, 30].

The inset of Fig. 2a shows a conventional topographic STM image. The location of the approximately circular graphite nanoflake can clearly be identified and the granular morphology of the Co and Au layers on top of the graphite and besides it can be seen. The graphite flake was 17 nm in height. The STM tip was positioned at the centre of the graphite flake, and the transmitted current was measured as a function of V_T for P and AP alignment of the Co and Ni₈₀Fe₂₀ magnetization (Fig. 2a). As expected [23–26], the transmission is nonzero only for $V_T < -0.8$ V when the electron energy is above the Au-Si Schottky barrier height. Most notably, the current is largest for the P state and more than a factor of three

smaller for the AP configuration. The large difference between I_C^P and I_C^{AP} with the graphite as spacer demonstrates efficient transmission of spin polarization through the graphite. This was further proven by measuring, with the STM tip still above the centre of the graphite nanoflake, the transmitted current while sweeping the magnetic field through a complete cycle from +100 Oe to -100 Oe and back (Fig. 2b, taken with constant tunnel current (3 nA) and tip bias (-1.8 V)). The magnetization of both ferromagnets was first saturated in a magnetic field of +100 Oe to obtain a P state yielding largest transmission (0.7-0.8 pA). When the magnetic field is swept to negative values, a transition to the AP state with lower transmission (0.2-0.3 pA) occurs due to magnetization reversal of the soft $\text{Ni}_{80}\text{Fe}_{20}$ layer, followed by a transition back to the P state around -40 Oe when the Co magnetization is also reversed. A similar behaviour is observed on the retrace, with hysteresis. The corresponding MC is $250 \pm 30\%$, demonstrating that a significant spin polarization is injected into the graphite and transmitted perpendicularly through the graphite spacer and its interfaces with the metals.

While the above results establish spin transport in graphite, a reliable quantitative analysis exploits the imaging capability of BEMM. This is required because of possible local variations of the transmitted current and the MC. The left two panels of Fig. 3 show a $0.6 \times 0.6 \mu\text{m}^2$ STM topography image and the corresponding height profile of the graphite nanoflake, which in this case is about 7 nm thick. The centre and right images are spatial maps of the transmitted current I_C for P and nominally AP state, respectively, all taken in the same area ($V_T = -1.8$ V). For the P state the transmitted current is largest and equal to about 0.25 pA per nA of injected tunnel current. For the image on the right, the current is strongly reduced in most of the area due to the AP alignment, and magnetic domain contrast appears in the left part, as often observed in BEMM on metal spin-valve stacks [22, 29]. However, the most important feature is that there is no significant difference in the transmission in the area with the graphite flake, as compared to the surrounding area without graphite. This applies to the P and to the AP state, as can be seen in the cross sections taken along a line intersecting the graphite flake (bottom panels). This leads to the following main quantitative conclusions: (i) the transmission through the graphite is nearly perfect, i.e., there is no significant attenuation of the current, and (ii), the MC with and without the graphite is identical, implying that the electrons are transmitted through the graphite and its interfaces without any measurable loss of spin polarization.

A similar set of data was obtained on the thicker graphite flake of 17 nm (Fig. 4, also for $V_T = -1.8$ V). Again, the transmission for P and AP state occurs without significant attenuation due to the graphite, and there is no reduction of the MC in the area where the additional graphite spacer is present (note that there are some small inhomogeneities at the edges of the graphite flake, causing strong attenuation of the hot-electron transmission for the P as well as the AP state (dark spots in the spatial maps of I_C)). More precise analysis is done using the distribution of current values across the images of Fig. 3 and 4 containing the 7 nm and the 17 nm thick graphite. The resulting histograms of the transmitted current are displayed in Fig. 5a and 5b, where the histograms in blue are obtained from the area with the graphite, while the red histograms correspond to the surrounding area without graphite. To first order, the histograms with and without graphite overlap, as expected from the images and cross sections already described. More precisely, the mean values of the transmitted current on the 7 nm flake are $I_C^P = 0.24 \pm 0.02$ pA/nA and $I_C^{AP} = 0.13 \pm 0.02$ pA/nA, whereas away from the graphite we have $I_C^P = 0.25 \pm 0.01$ pA/nA and $I_C^{AP} = 0.14 \pm 0.01$ pA/nA. Similarly, for the 17 nm graphite flake we have $I_C^P = 0.26 \pm 0.02$ pA/nA and $I_C^{AP} = 0.12 \pm 0.02$ pA/nA, and surrounding the flake we have $I_C^P = 0.255 \pm 0.01$ pA/nA and $I_C^{AP} = 0.12 \pm 0.01$ pA/nA.

As previously established [27], for hot electrons the current transmitted through a ferromagnet/spacer/ferromagnet stack can be described as a product of the transmissions of each layer if spin is conserved:

$$I_C^P \propto T_{NiFe}^M T_{Gr} T_{Co}^M + T_{NiFe}^m T_{Gr} T_{Co}^m, \quad (1)$$

$$I_C^{AP} \propto T_{NiFe}^M T_{Gr} T_{Co}^m + T_{NiFe}^m T_{Gr} T_{Co}^M, \quad (2)$$

where T^M and T^m denote the transmission of hot electrons of majority (M) and minority (m) spin in the ferromagnetic layers, and T_{Gr} is the transmission of the graphite (not spin dependent). All transmission factors depend exponentially on the layer thickness [27, 28]. Specifically, we have $T_{Gr} \propto e^{-d/\lambda_{k,E}}$, where d is the thickness of the graphite spacer and $\lambda_{k,E}$ is the length scale associated with the current attenuation due to *spin-conserving* scattering processes that change the energy or momentum of the hot electrons (not to be confused with the spin-relaxation length). Given that the transmission of the graphite is near unity (Fig. 5), we can conclude that the value of $\lambda_{k,E}$ must be at least on order of magnitude larger than the graphite thickness used. Hence, $\lambda_{k,E}$ is conservatively estimated

to be larger than 100 nm at 1.8 eV above the Fermi level. In materials where spin relaxation is dominated by scattering involving the spin-orbit interaction (Elliott-Yafet mechanism), there is an approximate scaling [1, 31] between the momentum scattering time τ and the spin-relaxation time τ_s . The ratio τ/τ_s depends on the spin-orbit interaction, and for materials with light elements (such as carbon) and weak spin-orbit interaction, we have $\tau/\tau_s \ll 1$, implying that many scattering events are needed to create a significant change of spin. Hence, the spin-relaxation length should be much larger than $\lambda_{k,E}$, and may thus approach the micron range. This is a rather surprising result for transport in the direction perpendicular to the graphene sheets, which are coupled in this direction by π orbitals with limited overlap. A much shorter spin scattering length was therefore expected, in analogy with spin transport via weakly interacting orbitals in organic materials, which yields spin-scattering lengths in the 10 to 40 nm range [7, 9–12]. Nevertheless, the spin-flip length for perpendicular transport in graphite is found to be significantly larger than the graphite thickness of up to 17 nm used here, and spin is thus essentially conserved. Note that transport parameters and spin-scattering lengths for hot electrons, as used here, are not the same as those of electrons at the Fermi energy. For hot electrons the carrier velocity is different (generally higher) compared to that of Fermi electrons, while the scattering cross section is also different (generally larger because of the larger phase space for elastic scattering and the additional inelastic scattering channels that are available for hot electrons).

Graphite can be obtained with high purity and hence is an ideal model system for a detailed investigation of spin transport across interfaces with weak electronic interactions, without the complications of impurities that are often present in organic compounds [4, 5]. This offers hope for a meaningful comparison with theoretical descriptions, for which our results provide a challenging benchmark. Also of particular interest in this regard is the recent theoretical prediction of strong spin filtering at crystalline interfaces between graphene/graphite and ferromagnets in perpendicular transport geometry [32, 33]. Combined with the perfect transmission of spin-polarized electrons through graphite, even at an energy of 1.8 eV, as demonstrated here, this raises prospects for graphite as a potential material for spintronics devices. The results also highlight the unique capability of our scanning-probe-based technique to study and directly visualize local spin transport in organic and carbon-based materials at the nanoscale.

Acknowledgement. We are grateful to Prof. P.J. Kelly and his team members for sharing their transport calculations, to Dr. R. Salvio for useful discussion on the sonication process, and to Prof. B.J. van Wees for his critical reading of the manuscript. This work was financially supported by the NWO-VIDI program and the Netherlands Nanotechnology Network NANONED (supported by the Ministry of Economic Affairs).

-
- [1] I. Žutić, J. Fabian and S. Das Sarma, *Rev. Mod. Phys.* **76**, 323, (2004).
 - [2] C. Chappert, A. Fert and F. Nguyen van Dau, *Nature Mater.* **6**, 813, (2007).
 - [3] W.J.M. Naber, S. Faez and W.G. van der Wiel, *J. Phys. D* **40**, R205, (2007).
 - [4] G. Szulczewski, S. Sanvito and M. Coey, *Nature Mater.* **8**, 693, (2009) and references therein.
 - [5] V. Dediu, L.E. Hueso, I. Bergenti and C. Taliani, *Nature Mater.* **8**, 707, (2009) and references therein.
 - [6] V. Dediu, M.Murgia, F.C. Matocotta, C. Taliani and S. Barbanera, *Solid State Commun.* **122**, 181, (2002).
 - [7] Z.H. Xiong, D. Wu, Z. Valy Vardeny and J. Shi, *Nature* **427**, 821, (2004).
 - [8] T.S. Santos, J.S. Lee, P. Migdal, I.C. Lekshmi, B. Satpati and J.S. Moodera, *Phys. Rev. Lett.* **98**, 016601, (2007).
 - [9] S. Pramanik, C.G. Stefanita, S. Patibandla, S. Bandyopadhyay, K. Garre, N. Harth and M. Cahay, *Nature Nanotech.* **2**, 216, (2007).
 - [10] J.H. Shim, K.V. Raman, Y.J. Park, T.S. Santos, G.X. Miao, B. Satpati and J.S. Moodera, *Phys. Rev. Lett.* **100**, 226603, (2008).
 - [11] M. Cinchetti, K. Heimer, J-P. Wustenberg, O. Andreyev, M. Bauer, S. Lach, C. Ziegler, Y. Gao and M. Aeschlimann, *Nature Mater.* **8**, 115, (2009).
 - [12] A.J. Drew, J. Hoppler, L. Schulz, F. L. Pratt, P. Desai, P. Shakya, T. Kreouzis, W. P. Gillin, A. Suter, N. A. Morley, V. K. Malik, A. Dubroka, K.W. Kim, H. Bouyanfif, F. Bourqui, C. Bernhard, R. Scheuermann, G. J. Nieuwenhuys, T. Prokscha and E. Morenzoni, *Nature Mater.* **8**, 109, (2009).
 - [13] K. Tsukagoshi, B.W. Alphenaar and H. Ago, *Nature* **401**, 572, (1999).

- [14] S. Sahoo, T. Kontos, J. Furer, C. Hoffmann, M. Grber, A. Cottet and C. Schenberger, *Nature Phys.* **1**, 99, (2005).
- [15] L.E. Hueso, J.M. Pruneda, V. Ferrari, G. Burnell, J.P. Valdes-Herrera, B.D. Simons, P.B. Littlewood, E. Artacho, A. Fert and N.D. Mathur, *Nature* **445**, 410, (2007).
- [16] N. Tombros, C. Jozsa, M. Popinciuc, H.T. Jonkman and B.J. van Wees, *Nature* **448**, 571, (2007).
- [17] M. Ohishi, M. Shiraishi, R. Nouchi, T. Nozaki, T. Shinjo and Y. Suzuki, *Jpn. J. Appl. Phys.* **46**, L605,(2007).
- [18] W.H. Wang, K. Pi, Y. Li, Y. F. Chiang, P. Wei, J. Shi and R. Kawakami, *Phys. Rev. B.* **77**, 020402, (2008).
- [19] S.P. Dash, S. Sharma, R.S. Patel, M.P. de Jong and R. Jansen, *Nature* **462**, 491, (2009).
- [20] P.A. Bobbert, W. Wagemans, F.W.A. van Oost, B. Koopmans and M. Wohlgenannt, *Phys. Rev. Lett.* **102**, 156604, (2009).
- [21] K. Matsubara, K. Sugihara and T. Tsuzuku, *Phys. Rev. B.* **41**, 969, (1990).
- [22] W.H. Rippard and R.A. Buhrman, *Appl. Phys. Lett.* **75**, 1001, (1999).
- [23] W.H. Rippard and R.A. Buhrman, *Phys. Rev. Lett.* **84**, 971, (2000).
- [24] E. Haq, H. Gokcan, T. Banerjee, F. M. Postma, M. H. Siekman, R. Jansen and J.C. Lodder, *J. Appl. Phys.* **95**, 6930, (2004).
- [25] W.J. Kaiser and L.D. Bell, *Phys. Rev. Lett.* **60**, 1406, (1988).
- [26] M. Prietsch, *Phys. Rep.* **253**, 163, (1995).
- [27] R. Jansen, *J. Phys. D: Appl. Phys.* **36**, R289, (2003).
- [28] R. Vlutters, O.M.J. van 't Erve, S.D. Kim, R. Jansen and J.C. Lodder, *Phys. Rev. Lett.* **88**, 027202, (2002).
- [29] E. Haq, T. Banerjee, M. H. Siekman, J. C. Lodder and R. Jansen, *Appl. Phys. Lett.* **86**, 082502, (2006).
- [30] T. Banerjee, E. Haq, M.H. Siekman, J.C. Lodder and R. Jansen, *Phys. Rev. Lett.* **94**, 027204, (2005).
- [31] J. Fabian and S. Das Sarma, *Phys. Rev. Lett.* **81**, 5624, (1998) and references therein.
- [32] V.M. Karpan, G. Giovannetti, P. A. Khomyakov, M. Talanana, A. A. Starikov, M. Zwierzycki, J. van den Brink, G. Brocks and P.J. Kelly, *Phys. Rev. Lett.* **99**, 176602, (2007).
- [33] V.M. Karpan, P. A. Khomyakov, A. A. Starikov, G. Giovannetti, M. Zwierzycki, M. Talanana,

G. Brocks, J. van den Brink and P.J. Kelly, Phys. Rev. B. **78**, 195419, (2008).

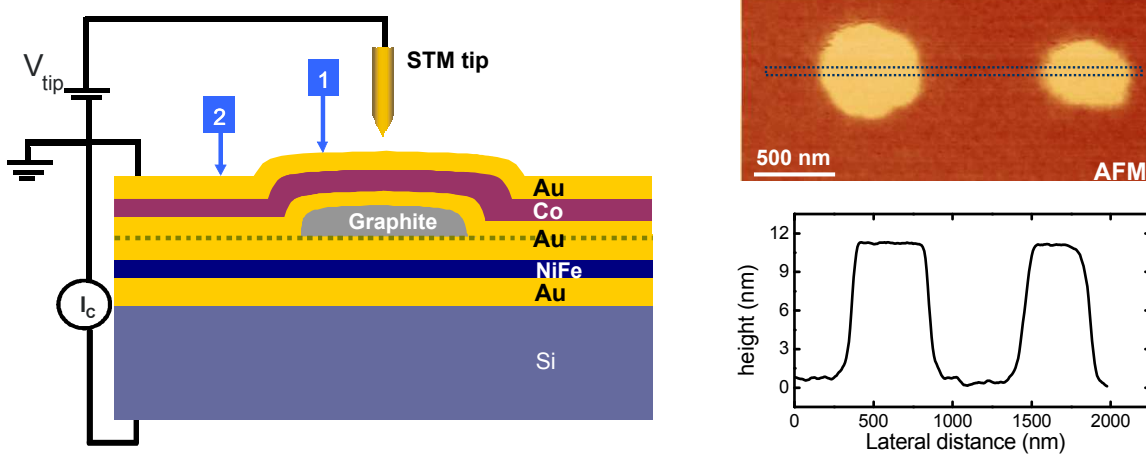


FIG. 1: (a) Schematics of the BEMM technique. The sample consists of a Si substrate coated with a layer stack of Au(8nm)/Ni₈₀Fe₂₀(3nm)/spacer/Co(3nm)/Au(4nm), where the spacer is either a graphite nanoflake sandwiched between two Au layers of 3 nm (location 1), or just 3+3 nm Au (location 2). The STM tip is used to locally inject electrons into the sample by tunneling at bias voltage V_T between tip and Au surface. The current I_C transmitted perpendicularly through the stack is collected in the Si with a third electrical contact. (b) AFM image of a complete sample structure (including the top metal coating), showing two graphite nanoparticles of approximately circular shape. (c) Height profile along the horizontal line intersecting both graphite flakes, as indicated in the image.

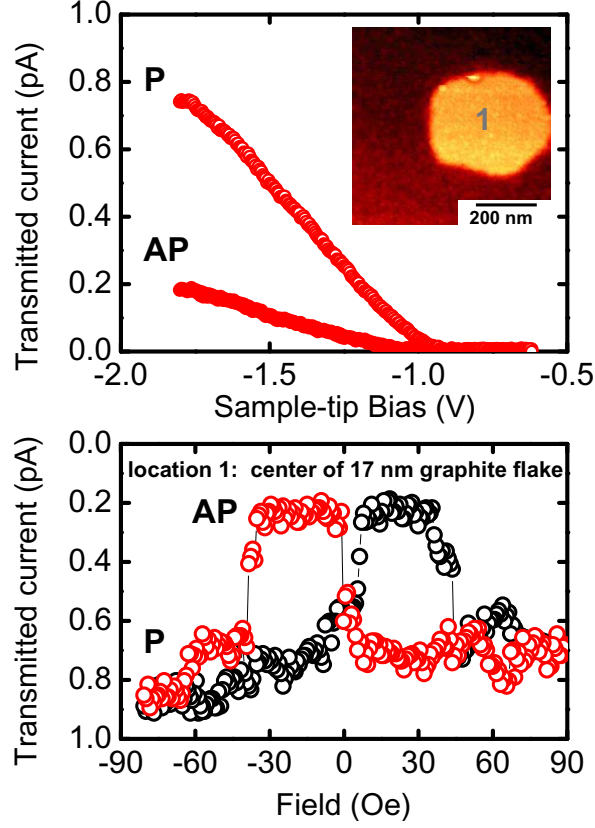


FIG. 2: (a) I_C versus V_T with the tip positioned at the centre of the 17 nm thick graphite flake (location 1). We first applied an in-plane magnetic field of -100 Oe, then reversed the field to $+20$ Oe (spectrum for AP state), and then increased the field to $+100$ Oe (spectrum for P magnetic state). The inset shows the $0.6 \times 0.6 \mu\text{m}^2$ topographic STM image (taken at $V_T = -1\text{V}$ and $I_T = 0.6$ nA) with location 1 indicated. (b) Local spin-valve measurement at the centre of the graphite flake (location 1), showing I_C versus magnetic field swept from negative to positive (black) or vice versa (red), at constant $V_T = -1.8\text{V}$ and $I_T = 3$ nA. $T = 150$ K.

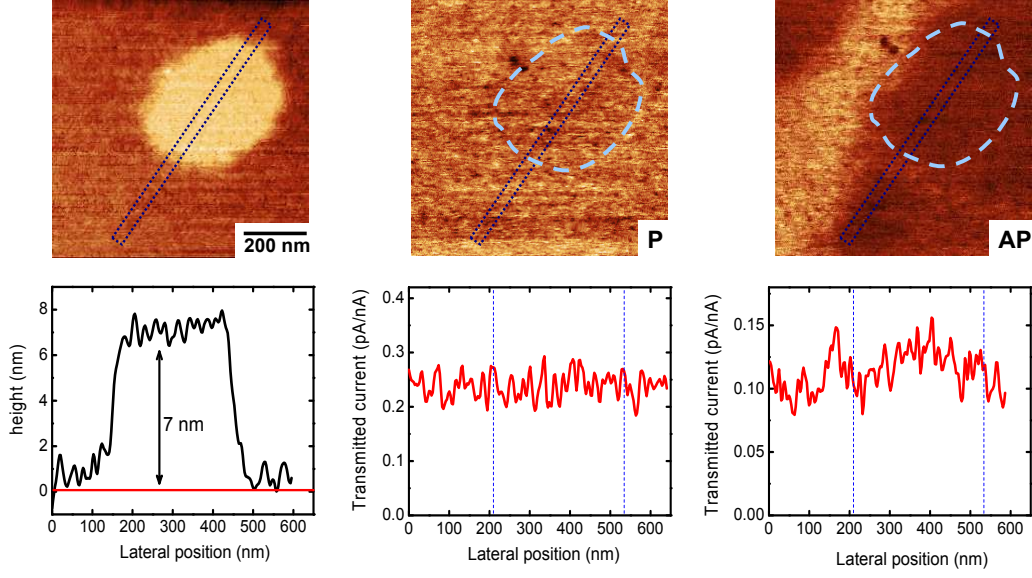


FIG. 3: Spatially resolved spin transmission through graphite spin-valve sandwiches. (a) Topographic STM image. (b) corresponding BEMM image of transmitted current I_C for +100 Oe magnetic field (P magnetic state). (c) BEMM image of I_C for nominally AP magnetic state, obtained by first setting the magnetic field to -100 Oe and then reversing it to $+20$ Oe. In the BEMM images, dark (bright) areas have low (high) transmitted current. (d,e,f) cross-section profiles of the signals along the line intersecting the graphite, as indicated in the images. Dashed lines in the cross-sections denote the boundary of the graphite flake. All data was obtained at $V_T = -1.8$ V and $I_T = 3$ nA in the same $0.6 \times 0.6 \mu\text{m}^2$ area containing a 7 nm high graphite flake. The rest of the layer stack is identical to that of Fig. 1. The transmitted current is given in pA/nA, as it is normalized to I_T . $T = 150$ K.

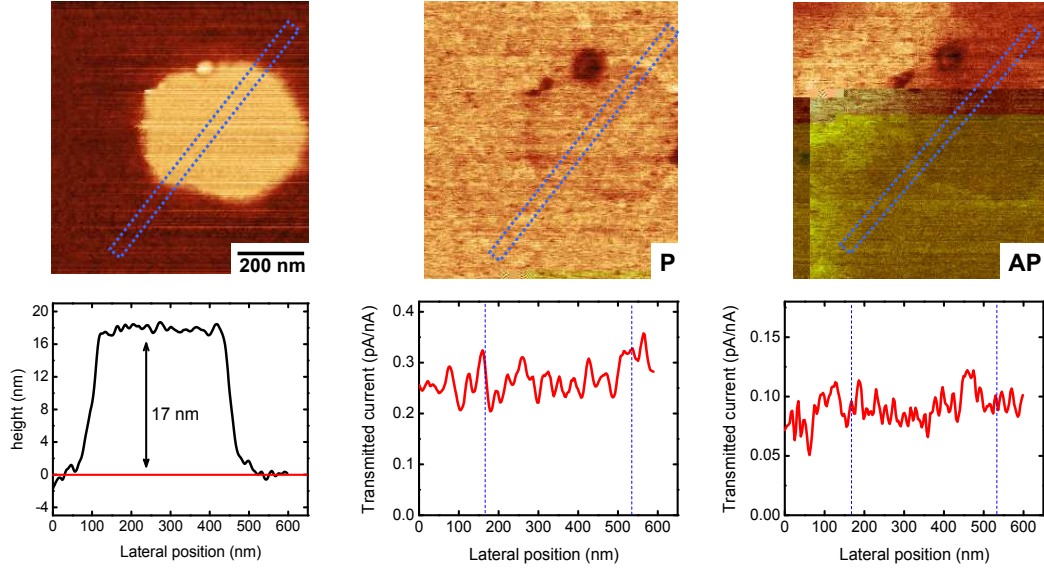


FIG. 4: Spatially resolved spin transmission through 17 nm of graphite. Similar set of data as shown in Fig. 3, obtained with exactly the same parameters, but in a region containing a 17 nm thick graphite flake (same flake as in Fig. 2(a),(b)).

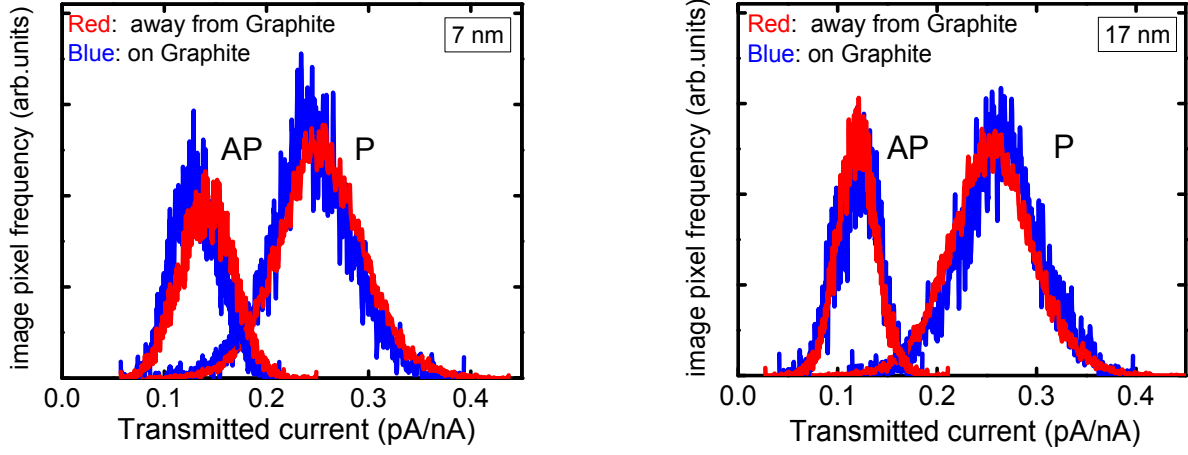


FIG. 5: Quantitative analysis using histograms of current distribution. (a) Histograms of the distribution of transmitted current for P and AP state, derived from BEMM images of Fig. 3 containing the 7 nm graphite flake. Histograms in blue are obtained from a square section of the image located fully within the boundary of the graphite flake, while histograms in red are obtained from an area not containing the graphite. The transmitted current is given in pA/nA, as it is normalized to I_T . Note that for the AP state, the left part of the images (containing magnetic domain contrast) was excluded from the analysis. (b) Similar set of histograms, but now derived from BEMM images of Fig. 4 containing the 17 nm graphite flake.